ELSEVIER

Effect of flow and temperature distribution on the performance of a PEM fuel cell stack

Jaewan Park, Xianguo Li *

Department of Mechanical Engineering, University of Waterloo, Waterloo, Ontario, Canada N2L 3G1

Abstract

A non-isothermal stack model has been developed to analyze the effects of flow variance and temperature distribution on the performance of a polymer electrolyte membrane (PEM) fuel cell stack. The stack model consists of the flow network solver for pressure and mass flow distributions for the reactant gas streams and cooling water, and the heat transfer solver for temperature distribution among the cells in the stack, as well as the fuel cell model for individual cell performance. Temperature, pressure and concentrations of fuel and oxidant are the most important conditions for the fuel cell operation. In this work, pressure, temperature and concentration distributions are determined incorporating the individual cell performance with the minor losses in stack flow network accounted for. The results indicate that the effect of temperature is dominant on the cell voltage variance when the flow variance is small for sufficiently uniform distribution of reactant flow among the cells in the stack. Sufficient flow uniformity can be achieved by a large manifold that reduces the cell active area, or a small flow channel diameter, the latter may result in excessive pumping power for the anode and cathode gas streams. The manifold and flow channel diameters were optimized considering stack performance and reactant stream pumping power requirement. It is further shown that the flow and temperature distribution have a different influence on the stack performance, and a judicial matching of their distribution can provide the ideal uniform cell voltage distribution. An optimal combination of the flow and temperature distribution along the stack yields the optimal stack performance.
© 2006 Elsevier B.V. All rights reserved.

Keywords: PEM fuel cell; Stack model; Flow network analysis; Temperature distribution; Thermal management; Stack cooling

1. Introduction

The greenhouse effect is currently considered as one of the most pressing environmental problems caused by the use of fossil fuels. Such environmental concern brought about the strong demand for clean power generation and fuel cell is receiving increasing attention as a clean power source, at least at the point of use. With its competitive power density and high efficiency as well as zero emission, the polymer electrolyte membrane (PEM) fuel cell has emerged as a promising alternative to internal combustion engine [1]. Cells are connected in series to form a fuel cell stack in order to satisfy the power demand of the practical applications. The performance degradation is known to be caused by the unequal supply of fuel and oxidant which results

in variations of each cell flow conditions for isothermal temperature distribution throughout the stack [2]. In reality, temperature variation along the stack has a significant impact on stack performance, which is known as the thermal management that remains one of the critical issues for PEM fuel cells. Therefore the stack performance must be analyzed based on the actual conditions present for each cell in the stack, which are influenced by the design and operating conditions of the stack. The optimization of stack design and operating parameters is necessary for improved performance and longer lifetime.

A considerable body of literature exists for the modeling and simulation of a single PEM fuel cell, as summarized in a recent review article [3]. Most of these analyses and modeling efforts can be categorized into three categories: the first is the empirical correlations for the cell performance with limited applicability and lack of predictive capability [4]; the second is the detailed CFD-based simulation [5–23]. These multi-dimensional CFD-based models impose significant computational penalty so that the models are limited to either over-simplified cell geome-

* Corresponding author.
  E-mail addresses: jwpark@engmail.uwaterloo.ca (J. Park),
x6li@uwaterloo.ca (X. Li).

Nomenclature

A_{cell}	active cell area (m^2)
A_f	flow path area (m^2)
C_f	wall friction coefficient
C_i	concentration of species i ($kmol\,m^{-3}$)
C_l	laminar wall friction coefficient
C_{min}	minimum heat capacity rate
C_p	heat capacity at constant pressure ($J\,K^{-1}$)
d_h	flow channel hydraulic diameter (mm)
D_h	manifold hydraulic diameter (mm)
E	voltage (V)
E_{rev}	reversible voltage (V)
E_{th}	thermoneutral voltage (V)
F	Faraday constant ($96{,}485\,C\,mol^{-1}$)
G	Gibbs free energy ($J\,N^{-2}\,m^{-3}$)
H	rate of heat transfer (kW)
J	cell current density ($A\,m^{-2}$)
l	distance from the manifold inlet (m)
L_{ch}	flow channel length (m)
L_m	manifold length (m)
$\dot{m}$	mass flow rate ($kg\,s^{-1}$)
n	exponent used to represent frictional/minor losses
$\dot{N}$	molar flow rate ($mol\,s^{-1}$)
N_{cell}	number of cells
N_{ch}	number of channels
N_l	number of loops in a stack ($N_{cell} - 1$)
$\dot{N}_R$	rate of reactant consumption in the catalyst layer ($mol\,s^{-1}$)
N_s	number of segment in a loop (6)
N_{turn}	number of turns in flow channel
$\dot{N}_0$	initially assumed molar flow rate ($mol\,s^{-1}$)
NTU	number of heat transfer unit
P	pressure (Pa)
Q	volume flow rate ($m^3\,s^{-1}$)
R	universal gas constant ($8.314\,kJ\,kmol^{-1}\,K^{-1}$)
r	flow resistance coefficient
Re	Reynolds number
S	entropy ($J\,K^{-1}$)
T	temperature (K)
T_h	temperature of heat source (K)
$T_{c,in}$	inlet temperature of cold stream (K)
U	overall heat transfer coefficient ($W\,m^{-2}\,K^{-1}$)
V	average velocity ($m\,s^{-1}$)

Greek letters

α	thermal diffusivity
Δ	difference
ε	effectiveness
ζ	stoichiometry
η	overpotential
θ	flow direction convention (+1 for clockwise, −1 for counter clockwise)
Θ	cell thickness (m)

Λ	bipolar plate effective height (m)
μ	viscosity ($N\,s\,m^{-2}$)
ρ	density ($kg\,m^{-3}$)
υ	kinematic viscosity
Ω	bipolar plate effective width (m)

Subscripts

A	anode
bp	bipolar plate
C	cathode
ch	flow channel
cell	fuel cell
drag	dragged molecules
e	electrode backing
f	friction
H^+	protons
H_2	hydrogen
i	loop number
in, inlet	in/inlet value
j	segment number
k	species number
l	laminar flow
loop	loop
m	manifold, membrane
max	maximum value
min	minimum value
out, outlet	out/outlet value
O_2	oxygen
ref	reference
R	reacting
stack	stack
t	turbulent flow
trans	transient flow condition
turn	total/turn
w	water as a coolant
0	initial/inlet value

tries (often for short straight flow channels) or over-simplified phenomena involved. For example, the entire PEM fuel cell (membrane-electrode assembly) was completely neglected from the computational domain [8], or more often the electrochemical reactions in the catalyst layers leading to power generation is either neglected completely or assumed to have infinitely large reaction rate, hence the entire catalyst layer, the heart and soul of fuel cells, is simplified into an infinitesimally thin mathematical surface—an unrealistic and simplistic approach. Because of the over-simplifications invoked in these models, sometimes artificial boundary conditions have to be invented, such as the fictitious water concentration [7]. Also due to the significant computational time required, these models are often limited to the investigation of specific phenomena occurring in the PEM fuel cell, such as electron transport [11,12], heat transfer [13], water transport [17,18], etc. It is clear that these CFD-based cell models are not suitable for the analysis and modeling of

PEM fuel cell stacks consisting of tens or hundreds of individual cells. The third category of the models available in the literatures [7,24] take into account both the electrochemical reactions in the catalyst layers (which are spatially resolved in the model), and the physical transport of reactant gas flows, product and process water, heat and the charged species in the individual cells and stacks, hence it is a fundamentally-based comprehensive approach, that provides the predictive capability with sufficiently accurate results. Further, the computational requirement is quite modest, thus it is selected for incorporation into the present stack model.

In contrast with the extensive single cell models available in literature, quite limited number of studies is available for the modeling and simulation of PEM fuel cell stacks. Thirumulai and White developed a performance model of a PEM fuel cell stack [25] by integrating a pipe flow network into the two-dimensional isothermal single cell model of Nguyen and White [26]. It has been shown that the voltage variation is caused by the unequal gas flow to the individual cells in an isothermal stack. In Baschuck and Li [2], the pressure and mass flow rates were obtained from a hydraulic model and was used as operating conditions for their cell model [27]. The effect of stack manifold size and the number of gas flow channels per bipolar plate on the variance of cell performances was investigated as well. Karimi et al. [28] conducted an extensive work on optimization of the stack configuration using flow network model along with the cell model of Baschuk and Li [27]. The minor pressure loss caused by complicated flow patterns in stack was shown to have considerable impact, and the multiple inlets for the stack manifold were suggested to increase the flow uniformity of the flow channels in each cell.

There exist only few results that deal with the thermal management in the fuel cell stack. Maggio et al. [29] investigated the temperature and current density distribution using a three-dimensional model. The temperature in the cooling plate, cooling water and membrane electrode assembly (MEA) was found through application of conservation of energy, while the cell performance was determined with the empirical relation of Patel et al. [30]. Using empirical model of Kim et al. [31], Lee and Lark carried out a numerical simulation for the thermo-physical behavior of fuel cell stack [32]. The entire fuel cell system including oxidant supply and cooling pump was modeled in Barbir et al. [33] with empirical linear voltage relationship.

In this work, a non-isothermal stack model has been developed to analyze and optimize the PEM fuel cell stack performance. The model consists of a flow network model for the thermal and physical behavior of the reactant streams for the stack flow configuration investigated, a thermal model for the temperature distribution throughout the stack and a fuel cell model based on Baschuk and Li [27] for the individual cell performance. The pressure, temperature and flow distributions for the fuel, oxidant and coolant streams in the stack are obtained by incorporating cell performance, heat generation and transport phenomena. The heat transfer to the fuel, oxidant and coolant streams are analyzed and the effects of temperature distribution on the stack performance are investigated. The performance of the stack is evaluated for different stack design and operating conditions.

2. Mathmatical models

2.1. Stack flow model

Fig. 1 shows a schematic drawing of a PEM fuel cell stack in which cells are combined in series to generate sufficient power for practical application. The individual cell consists of a membrane electrolyte assembly (MEA) sandwiched between two bipolar plates. The electrode backings, catalyst layers and polymer electrolyte membrane are referred to as MEA where direct current is produced. In each cell, fuel and oxidant are supplied to both sides of MEA through the flow channels on the bipolar plates. The electron is generated in the anode catalyst layer through oxidation and consumed in the cathode catalyst layer by reduction. The polymer electrolyte membrane conducts the pro-

① Coolant Channel
② Bipolar Plate (Gas Flow Channel)
③ Electrode Backing Layer
④ Catalyst Layer
⑤ Polymer Electrolyte Membrane Layer
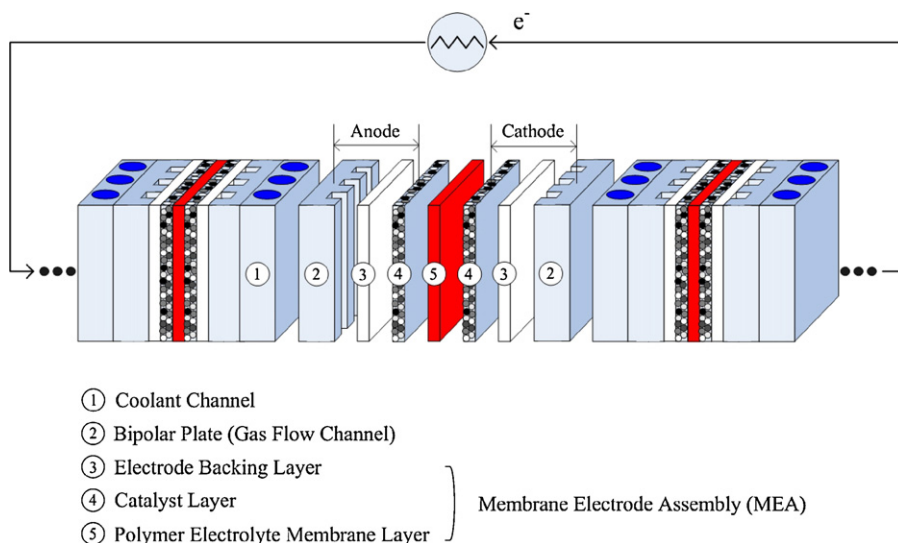} Membrane Electrode Assembly (MEA)

Fig. 1. Schematic of a polymer electrolyte membrane fuel cell stack.

ton produced by hydrogen oxidation to the cathode. Electrode backing and bipolar plates are conductive to deliver electrons from one cell to the next. To remove the heat produced by a PEM fuel cell, liquid water flows as a coolant through cooling path. An additional plate is inserted to provide coolant path between each cell or the cooling path could be integrated in the bipolar plate. Hydrogen and oxygen are supplied to each cell through the intake manifolds while excess reactants and reaction product exit to the exhaust manifolds. The electrochemical reaction starts at the inlet of flow channel and continues downstream while the chemical energy is converted into electrical energy, producing heat and water at the same time. The gas flow channels remove the water within the MEA and also supply the humidity required to prevent polymer electrolyte membrane dehydration.

Fig. 2 shows a flow network for the present model development. In order to obtain the pressure, stoichiometry, and reactant composition for each cell, the mass flow rate and pressure distributions within the stack must be determined; this constitutes the stack flow model. Flow channels on bipolar plate are modeled as up and downstream segments with one reaction site where the electro-chemical reaction and heat transfer occur. Flow channels are connected by intake and exhaust manifolds constituting a stack flow network. The flow configuration is assumed to be identical for the fuel, oxidant and coolant streams in this work. Only heat transfer occurs for the coolant stream while heat and mass transfers occur simultaneously for the other two streams. The pressure, temperature, and compositions are assumed to be uniform in each of the loop segment. The inlet hydrogen and oxygen molar flow rates to the anode and cathode are determined according to stoichiometry:

$$\dot{N}_{H_2} = \frac{\zeta_A N_{cell} J A_{cell}}{2F} \tag{1}$$

$$\dot{N}_{O_2} = \frac{\zeta_C N_{cell} J A_{cell}}{4F}, \tag{2}$$

where ζ_A and ζ_C are the anode and cathode stoichiometries, N_{cell} the number of cells in the stack, J the current density, A_{cell} the active area of the cell, and F is the Faraday constant. The inlets of the anode and cathode intake manifolds are saturated with water vapor for the present simulation. The total flow rates are obtained by adding the amount of water vapor to that of hydrogen for the anode stream and by adding the amount of water and nitrogen to that of oxygen for the cathode stream. The mass must be conserved at every node except at the reaction site. The rate of hydrogen production at the reaction site depends on the current density and it is calculated using Faraday's law:

$$\Delta \dot{N}_{R,H_2} = -\frac{J A_{cell}}{2F} \tag{3}$$

where the negative sign represents the fact that hydrogen is actually consumed at the reaction site. It is assumed that the exit stream of the anode is fully saturated and the excess water is migrated through the polymer electrolyte membrane as a net result of electroosmotic drag and back diffusion. The total consumption rate in the anode reaction site can be written as
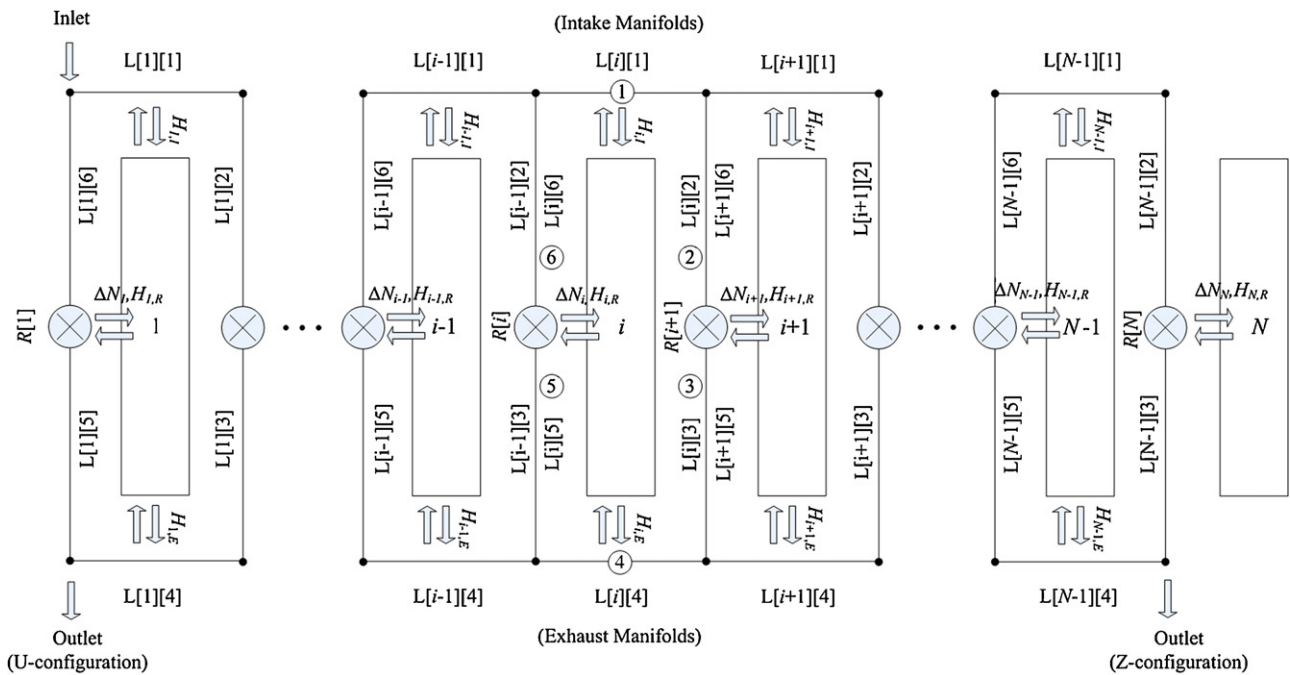
$H_{i,IRE}$: The amount of heat transfer at i^{th} loop (I: to the intake manifold, R: to the reaction site, E: to the exhaust manifold)
$L[i][j]$: A loop segment in flow network (i: loop number, j: loop segment number)
N : Number of cell
ΔN_i : The amount of reaction at i^{th} loop (positive for anode, negative for cathode)
$R[i]$: A reaction site at i^{th} loop

Fig. 2. A flow network diagram of heat and mass transfer in a PEM fuel cell stack; numbers (1)–(6) represent the loop segment number at ith loop.

follows:

$$\Delta \dot{N}_A = \Delta \dot{N}_{R,H_2} + \dot{N}_{drag,H_2O} \tag{4}$$

where $\dot{N}_{drag,H_2O}$ is the net water transport from the anode to the cathode through the electrolyte membrane. In cathode catalyst layer, oxygen is consumed and water molecule is produced by the chemical reaction. The resultant composition at the exit of reaction site as, considering the amount of dragged water molecule:

$$\Delta \dot{N}_C = \Delta \dot{N}_{R,O_2} + \Delta \dot{N}_{R,H_2O} + \dot{N}_{drag,H_2O} \tag{5}$$

The production rate of oxygen, $\Delta \dot{N}_{R,O_2}$, and the production rate of water, $\Delta \dot{N}_{R,H_2O}$, are given as

$$\Delta \dot{N}_{R,O_2} = -\frac{JA_{cell}}{4F} \tag{6}$$

$$\Delta \dot{N}_{R,H_2O} = \frac{JA_{cell}}{2F} \tag{7}$$

Water condensation may occur as the amount of water increases in the cathode. Hence, four species may exist at the cathode channel exit, including oxygen, liquid water, water vapor and nitrogen.

In Fig. 2, two adjacent gas flow channels and a pair of intake and exhaust manifolds constitute a closed loop around a MEA. The loop segment is numbered clockwise starting from the intake manifold as shown in Fig. 2. The pressure changes around the ith closed loop should be zero to satisfy the conservation of energy, i.e.

$$\sum_{j=1}^{N_s} \theta_{i,j} \Delta P_{i,j} = 0 \quad (i = 1, 2, 3, \ldots, N_l) \tag{8}$$

where j is a segment number, N_s the number of segments in a loop, $\theta_{i,j}$ a sign convention for the flow direction, $\Delta P_{i,j}$ the amount of pressure drop at the segment j in ith loop and N_l is the total number of loops in a stack. In any closed loop, $\theta_{i,j}$ is considered to be 1 for the clockwise and -1 for counterclockwise flow. The pressure drop caused by frictional loss on the inside wall of flow channel is estimated based on Darcy–Weisbach equation:

$$\Delta P_{i,j} = C_{f,i,j} \frac{L_{i,j}}{D_{h,i,j}} \frac{\rho_{i,j} V_{i,j}^2}{2} \tag{9}$$

where $L_{i,j}$ is the length of loop segment, $D_{h,i,j}$ the hydraulic diameter, $\rho_{i,j}$ the fluid average density, and $V_{i,j}$ the flow speed, and $C_{f,i,j}$ is the friction coefficient determined from the following correlation:

$$C_{f,i,j} = \begin{cases} C_1/Re_{D_{h i,j}} & Re_{D_{h i,j}} < 2 \times 10^3 \\ 0.316/Re_{D_{h i,j}}^{1/4} & 4 \times 10^3 < Re_{D_{h i,j}} < 10^5 \end{cases} \tag{10}$$

where C_1 is a constant depending on the flow path geometry. The Reynolds number in Eq. (10) is defined based on the hydraulic diameter of each loop segment wth $\mu_{i,j}$ representing average viscosity:

$$Re_{i,j} = \frac{\rho_{i,j} V_{i,j} D_{h,i,j}}{\mu_{i,j}} \tag{11}$$

The value of $C_{f,i,j}$ is linearly interpolated for the value of $Re_{i,j}$ between 2000 and 4000. In the anode and cathode streams, the volume flow rate is obtained based on the ideal gas law as follows:

$$Q_{i,j} = \sum_k \frac{\dot{N}_{k,i,j} RT}{P_{k,i,j}} \tag{12}$$

where k is the species number, $\dot{N}_{k,i,j}$ and $P_{k,i,j}$ are the molar flow rate and partial pressure of the species k, respectively. The volume of the condensed liquid water is neglected in anode and cathode downstreams. The thermal properties of species are determined based on the absolute temperature and then the averages are calculated according to compositions following Baschuck and Li [2].

The mass balance is applied to the every node in the intake manifold, reaction site, and exhaust manifold. Since each closed loop shares the vertical loop segments with adjacent closed loop, e.g. $L[i]$ [2] is equivalent to $L[i+1]$ [6] in Fig. 2, the mass balance for the vertical loop segment is expressed in terms of the mole flow rate as

$$\dot{N}_{i,1} = \frac{\theta_{i-1,1} \dot{N}_{i-1,1} - \theta_{i-1,2} \dot{N}_{i-1,2} (+\dot{N}_{inlet})}{\theta_{i,1}} \tag{13}$$

$$\dot{N}_{i,5} = \frac{\theta_{i,6} \dot{N}_{i,6} - \Delta \dot{N}_i}{\theta_{i,5}} \tag{14}$$

$$\dot{N}_{i,4} = \frac{\theta_{i-1,3} \dot{N}_{i-1,3} - \theta_{i-1,4} \dot{N}_{i-1,4} (-\dot{N}_{outlet})}{\theta_{i,4}} \tag{15}$$

where $\Delta \dot{N}_i$ is the molar flow rate of reaction, and $\dot{N}_{inlet}$ and $\dot{N}_{outlet}$ are the molar flow rates entering and leaving the fuel cell stack to be considered only at the stack inlet and outlet position. A negative flow rate during iteration indicates that the flow direction in a loop segment is incorrect and must be reversed. The conservation of energy requires that the summation of pressure drop around any closed loop in Fig. 2 should be equal to zero. The pressure drop in a loop segment is contributed by frictional and minor losses, and is related to the flow rate:

$$\Delta P_{i,j} = \theta_{i,j} [r_{1,i,j} Q_{i,j}^{n_{i,j}} + (r_{2,i,j} + r_{3,i,j}) Q_{i,j}] \tag{16}$$

where $r_{1,i,j}$ is the coefficient of frictional loss, $r_{2,i,j}$ the coefficient of divergence (confluence) loss between intake (exhaust) manifold and flow channel, and $r_{3,i,j}$ is the coefficient of bending loss in serpentine flow channel. The exponent, $n_{i,j}$, is dependent on the flow condition: 1 for laminar flow and 1.75 for turbulent flow. $r_{1,i,j}$ in Eq. (16) can be expressed for the jth segment in ith loop, as follows:

$$r_{1,i,j} = \begin{cases} \dfrac{C_{f,l} L_{i,j} \mu_{i,j}}{2.0 A_f D_{h,i,j}^2} & Re_{D_{h i,j}} < 2 \times 10^3 \\ \dfrac{0.158 L_{i,j} \mu_{i,j}^{0.25} \rho_{i,j}^{0.75}}{D_{h,i,j}^{1.25} A_f^{1.75}} & 4 \times 10^3 < Re_{D_{h i,j}} < 5 \times 10^5 \end{cases} \tag{17}$$

Correlations for $r_{2,i,j}$ and $r_{3,i,j}$ depending on the flow configurations are given in Table 1 [34].

2.2. Fuel cell model

The efficiency of a fuel cell is degraded as waste heat is produced due to the irreversibility of electro-chemical reaction and in the transport of reactants, electrons and protons in the cell. The amount of heat produced is equivalent to the residue of the maximum available chemical energy after producing electricity. In this model, the amount of heat in each cell is estimated from the difference between the thermoneutral voltage and cell output voltage:

$$H_{i,\text{total}} = JA(E_{\text{th},i} - E_{\text{cell},i}) \tag{18}$$

where $E_{\text{th},i}$ is the thermoneutral voltage and $E_{\text{cell},i}$ is the cell voltage. The thermoneutral voltage is a property of the fuel defined as

$$E_{\text{rev}} = \frac{\Delta H}{nF} \tag{19}$$

The individual cell voltage in the stack is determined using the single cell model developed by Baschuk and Li [27], and is obtained from the reversible cell voltage E_{rev} and the overpotentials occurring in the various components of the PEM fuel cell as follows:

$$E_{\text{cell}} = E_{\text{rev}} - \eta_{\text{a}} - |\eta_{\text{c}}| - 2\eta_{\text{bp}} - 2\eta_{\text{e}} - \eta_{\text{m}} \tag{20}$$

where η_{a} and η_{c} are the overpotentials attributed to the anode and cathode catalyst layers, respectively. The voltage losses caused by the bipolar plate, electrode backing and polymer electrolyte membrane are denoted by η_{bp}, η_{e} and η_{m}, respectively. The voltage losses attributed to the bipolar plate is calculated by considering the electrode backing and bipolar plate as electrical resistances. The overpotential associated with the proton migration in the polymer electrolyte membrane is determined by the Nernst–Planck equation assuming a constant conductivity for the fully hydrated polymer electrolyte membrane. The anode and cathode catalyst layer overpotentials are found by considering species conservation, and proton and electron migration within the catalyst layers. Proton and electron migration through the catalyst layers are related to the protonic and electrical current using Ohm's law. Species conservation requires modeling of reaction kinetics and mass transport. Oxygen reduction is modeled with the Butler–Volmer equation in the cathode catalyst layer. The reversible voltage, E_{rev}, is calculated from a modified Nernst equation with extra terms to account for the deviation from the standard reference temperature and concentration:

$$E_{\text{rev}} = \frac{\Delta G}{2F} + \frac{\Delta S}{2F}(T - T_{\text{ref}})$$
$$+ \frac{RT}{2F} \ln\left[\left(\frac{C_{\text{H}_2}}{C_{\text{H}_2,\text{ref}}}\right)\left(\frac{C_{\text{O}_2}}{C_{\text{O}_2,\text{ref}}}\right)^{1/2}\right] \tag{21}$$

where ΔG is the change in Gibbs free energy, ΔS the change in entropy, R the universal gas constant, T the absolute temperature of the MEA, and C_i denotes the concentration of species i at the electrode backing/catalyst layer in mol m^{-3}. The reference value of temperature, T_{ref}, is 298.15 K while the reference concentrations for hydrogen and oxygen are 22.22 and 7.033 mol m^{-3} respectively. The reference concentrations represent the concen-

Table 1
Branch, confluence, and bend head loss correlations [34]

Configuration	Correlations
Diverging T	$\Delta P_{1,j} = k_{1-j}\frac{\rho_1 V_1^2}{2}$ ($j = 2, 3$) $k_{1-2} = \left[a_1 + a_2\left(\frac{V_2}{V_1}\right) + a_3\left(\frac{V_2}{V_1}\right)^2\right]\frac{1}{Re_2^{b_1}}\left(\frac{V_2}{V_1}\right)^2$ $k_{1-3} = \frac{a_4}{Re_2^{b_2}}\left(\frac{V_3}{V_1}\right)^2$
Converging T	$\Delta P_{1,j} = k_{1-j}\frac{\rho_1 V_1^2}{2}$ ($j = 2, 3$) $k_{1-2} = \left[a_1 + a_2\left(\frac{V_1}{V_2}\right) + a_3\left(\frac{V_1}{V_2}\right)^2\right]\frac{1}{Re_2^{b_1}}\left(\frac{V_1}{V_2}\right)^2$ $k_{1-3} = \frac{a_4}{Re_2^{b_2}}\left(\frac{V_3}{V_2}\right)^2$
Bending	$\Delta P_{\text{bend}} = k\frac{\rho v^2}{2}$ $k = k_{\text{loc}} + k_{\text{fr}}$ $k_{\text{loc}} = \frac{0.21}{(R_0/d_{\text{h}})^{0.25}}$ (90° bend, square duct) $k_{\text{fr}} = 0.0175\frac{R_0}{d_{\text{h}}}\delta\lambda$ (δ in degrees) $\lambda = 32\left(Re_{d_{\text{h}}}\sqrt{\frac{2R_0}{d_{\text{h}}}}\right)^{-2/3}$ (laminar)

tration of hydrogen and oxygen in Nafion at a temperature of 298.15 K and partial pressure of 1 atm.

2.3. Heat transfer model

Within the framework of the present analysis, each cell can be considered as a parallel flow heat exchanger in which heat is transferred from the MEA to the fuel, oxidant and coolant streams. The pressure, temperature and flow rates of the streams must be obtained incorporating individual cell operation since the thermal and physical flow conditions and the individual cell performance are dependent on each other. In this work, the effectiveness-NTU method is applied to determine the amount of heat transfer and the temperature of the each loop segment. The log mean temperature difference (LMTD) method is not eligible for the present study since the unknown values are not only the outlet temperature but also the temperature of the heat source (i.e. the temperature of MEA). The analysis is based on the following assumptions:

1. The individual MEA has a uniform temperature.
2. The reactant flow and thermal conditions are fully developed, neglecting the entrance effect.
3. Thermal resistances at the surface of the flow channel including fouling effects are negligible.
4. The convective heat transfer on the outside surface of the fuel cell stack is negligible.

The number of heat transfer unit (NTU) is a dimensionless parameter that is widely used for the heat exchanger analysis

and is defined as

$$NTU = \frac{UA}{C_{min}} \tag{22}$$

where U is the overall heat transfer coefficient, A the area of heat transfer and C_{min} is the minimum heat capacity rate. The overall heat transfer coefficient is equivalent to the heat transfer coefficient h since conduction and other thermal resistances are neglected. The value of h is obtained from

$$h = \frac{k}{D_h} Nu_{D_h} \tag{23}$$

and the Nusselt number is determined from the following correlations for the internal flow [35]:

$$Nu_{D_h} = \begin{cases} 3.66 & Re_{D_h} < 2000, \; Pr > 0.6 \\ 0.023 \, Re_{D_h}^{4/5} \, Pr^{0.4} & Re_{D_h} > 10000, \; Pr > 0.6) \end{cases} \tag{24}$$

where Pr is the Prandtl number in each loop segment, defined as:

$$Pr = \frac{\nu}{\alpha} \tag{25}$$

where ν is the kinematic viscosity and α is the thermal diffusivity. The Nusselt number of 3.66 for the laminar flow is based on constant surface temperature, consistent with the assumption of the uniform temperature in MEA [35]. The Nusselt number within the transition flow condition, $2000 < Re_{D_h} < 10,000$, is linearly interpolated. The value of the effectiveness, ε, in each
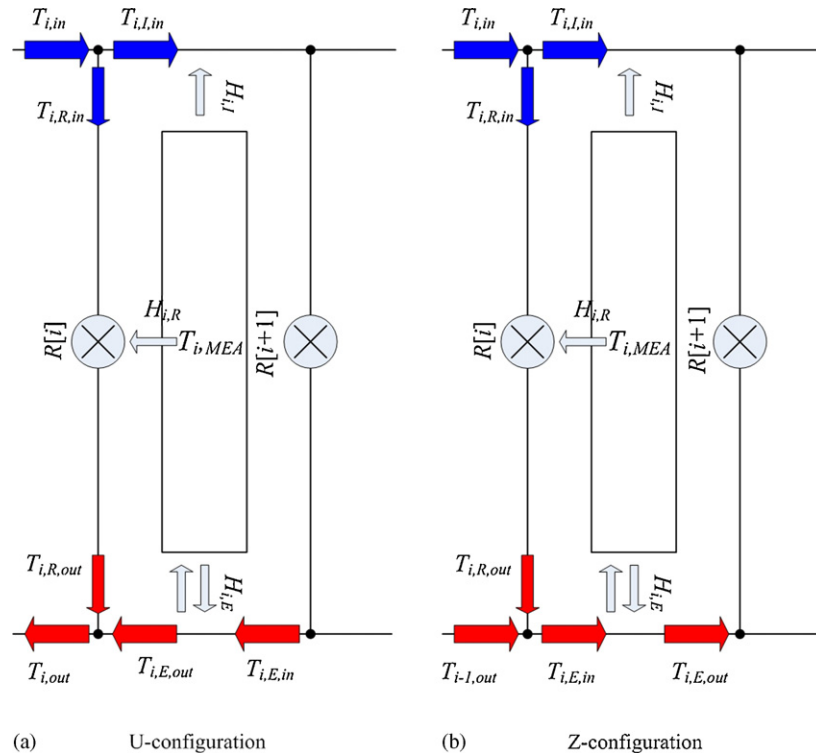

Fig. 3. Schematic of temperature distribution and heat transfer in the flow network.

flow loop segment can be found according to the following correlation against the constant temperature heat source:

$$\varepsilon = 1 - \exp(-\text{NTU}) \tag{26}$$

The amount of heat transfer is proportional to the effectiveness, the heat capacity rate, and the temperature difference between the MEA and any other flow:

$$H = \varepsilon C_{\min}(T_h - T_{c,\text{in}}) \tag{27}$$

where $C_{\min}$ is the minimum heat capacity rate, T_h the temperature of the heat source and $T_{c,\text{in}}$ is the inlet fluid temperature of the cold stream, respectively.

Fig. 3 is given to elucidate the mathematical scheme for the temperature distribution and the heat transfer in U and Z configuration. The temperature of the MEA and the amount of heat transfer to the intake manifold, reaction site, and exhaust manifold is determined from the given inlet temperature and the total amount of heat generated, $H_{\text{total},i}$. At steady sate, the heat generated in each MEA is discharged completely so that the temperature of the MEA will remain unchanged. By applying the energy and mass conservation at each node in Fig. 3(a), the

following equations are obtained for the U configuration stack:

$$T_{i,\text{R,in}} = T_{i,\text{in}} \tag{28}$$

$$T_{i,I,\text{in}} = T_{i,\text{in}} \tag{29}$$

$$T_{i,\text{R,out}} = T_{i,\text{R,in}} + \frac{H_{i,\text{R}}}{\dot{m}_{i,\text{R}}C_{p,i,\text{R}}} \tag{30}$$

$$T_{i,\text{out}} = \frac{\dot{m}_{i,\text{R}}C_{p,i,\text{R}}T_{i,\text{R,out}} + \dot{m}_{i,\text{E,out}}C_{p,i,\text{E}}T_{i,\text{E,out}}}{\dot{m}_{i,\text{out}}C_{p,i,\text{out}}} \tag{31}$$

The amount of heat transfer rate to the intake manifold, reaction site, and exhaust manifold can be estimated as follows:

$$H_{i,I} = \varepsilon_{i,I}\dot{m}_{i,I}C_{p,i,I}(T_{i,\text{MEA}} - T_{i,I,\text{in}}) \tag{32}$$

$$H_{i,\text{R}} = \varepsilon_{i,\text{R}}\dot{m}_{i,\text{R}}C_{p,i,\text{R}}(T_{i,\text{MEA}} - T_{i,\text{R,in}}) \tag{33}$$

$$H_{i,\text{E}} = \varepsilon_{i,\text{E}}\dot{m}_{i,\text{E}}C_{p,i,\text{E}}(T_{i,\text{MEA}} - T_{i,\text{E,in}}) \tag{34}$$

The total amount of heat should be equivalent to the summation of above three terms as

$$H_{i,I} + H_{i,\text{R}} + H_{i,\text{E}} = H_{i,\text{total}} \tag{35}$$

The unknown variables are $T_{i,I,\text{in}}$, $T_{i,\text{R,in}}$, $T_{i,I,\text{out}}$, $H_{i,I}$, $H_{i,\text{R}}$, $H_{i,\text{E}}$, $T_{i,\text{out}}$, $T_{i,\text{E,out}}$ and $T_{i,\text{MEA}}$ in Eqs. (28)–(35). The temperature
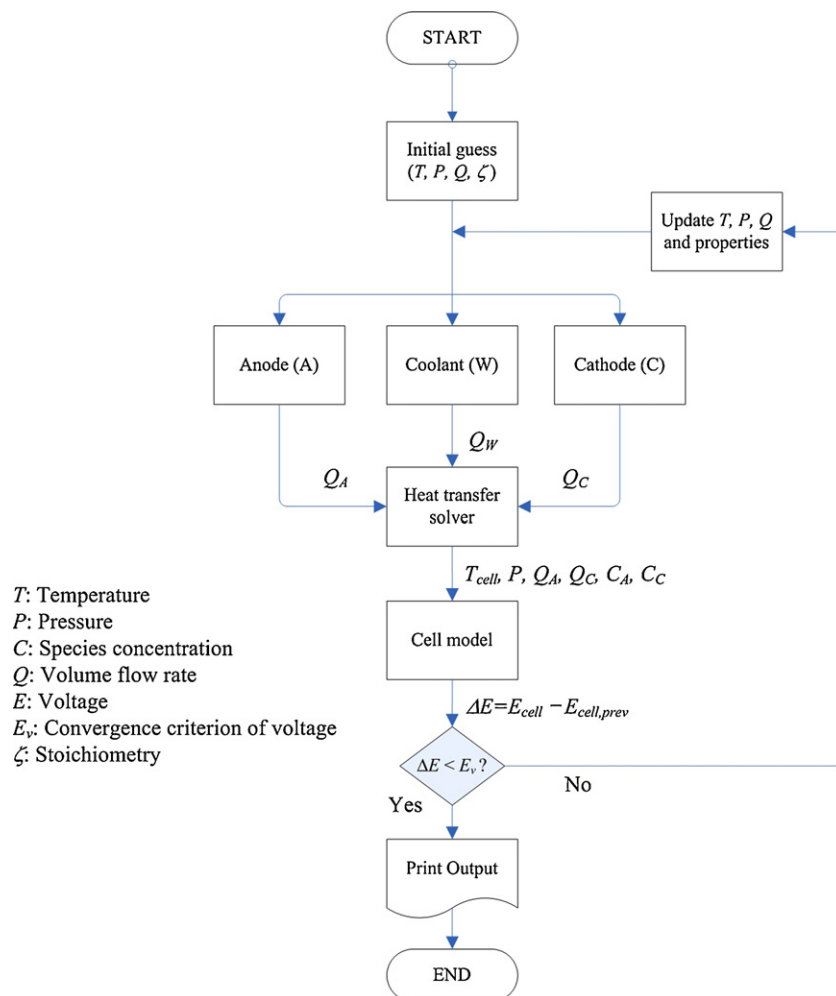

Fig. 4. A flow chart of the stack model.

distribution and the amount of heat transfer are determined from the first cell. For the first cell in U configuration stack, $T_{i,\text{out}}$ corresponds to the temperature of the coolant out of the stack, therefore it can be estimated from the total heat generation of the stack as follows:

$$T_{1,\text{out}} = T_{1,\text{in}} + \frac{\sum_{i=1}^{N} H_{i,\text{total}}}{\dot{m}_{\text{total}} C_{p,\text{out}}} \tag{36}$$

Similarly for Z configuration stack, Eq. (31) is replaced by

$$T_{i,\text{E,in}} = \frac{\dot{m}_{i,\text{R}} C_{p,i,\text{R}} T_{i,\text{R,out}} + \dot{m}_{i-1,\text{E,out}} C_{p,i-1,\text{E}} T_{i-1,\text{E,out}}}{\dot{m}_{i,\text{E}} C_{p,i,\text{E}}} \tag{37}$$

where $T_{i,\text{E,in}}$ equals to $T_{i,\text{R,out}}$ for the first cell since $T_{i-1,\text{out}}$ does not exist at the first cell for Z configuration. A set of linear Eqs. (28)–(35) can be solved analytically or an iterative solution can be found by modifying the temperature of the MEA until Eq. (35) is satisfied. The mathematical scheme for the anode and cathode gas streams is similar to that of the coolant stream. For fast convergence, the heat transfer to the anode and cathode streams is neglected for the first iteration. Since coolant water has much larger heat capacity compared to the other two-reactant gas streams, most of heat generated in the MEA should be transferred to the coolant stream. The amount of heat transfer to the anode and cathode is estimated by Eqs. (32)–(34) considering the heat of water condensation.

3. Numerical procedures

Fig. 4 shows a flow diagram of the present stack model. The stack model consists of three major modules: a flow solver, a heat transfer solver, and a fuel cell module. In the flow solver, pressure and flow rates of species for the anode, cathode, and coolant streams are obtained according to the given inlet conditions. The flow solver is based on the Hardy Cross method which needs an iterative procedure to find pressure and flow rate distributions in a flow network [36]. Starting from an assumed flow rate in each segment of all the loops, the flow rate of each loop segment is modified observing the mass and energy conservation until a converged flow distribution is found. With $Q_{i,j,\text{prev}}$ being the volume flow rate of the previous iterative step, the flow rate is corrected as

$$Q_{i,j} = Q_{i,j,\text{prev}} + \Delta Q_i \tag{38}$$

Table 2
Parameters and properties used in the present PEM fuel cell stack simulations

| Component	Parameter	Value
Bipolar plate	Width (Ω)	12×10^{-2} m
	Height (Λ)	12×10^{-2} m
	Thickness (Θ)	0.012 m
Gas flow channel (anode, cathode)	Channel length (l_{ch})	3.0×10^{-1} m
	Number of channel (N_{ch})	10
	Number of U-turn (N_t)	3–8
	Hydraulic diameter (d_{h})	0.75–2.25 mm
	Manifold hydraulic diameter (D_{h})	12.5–20.0 mm
	Gas inlet temperature (T_{in})	353.15 K
Coolant path	Path length ($l_{\text{ch,w}}$)	3.0×10^{-1} m
	Hydraulic diameter ($d_{\text{h,w}}$)	1.5 mm
	Number of channel ($N_{\text{ch,w}}$)	10
	Number of turn ($N_{\text{t,w}}$)	3
	Manifold hydraulic diameter ($D_{\text{h,w}}$)	20.0 mm
	Coolant inlet temperature ($T_{\text{in,w}}$)	353.15 K
	Coolant flow rate (Q_{w})	0.85×10^{-4} to 2.84×10^{-3} m^3 s^{-1}
	Reynolds number ($Re_{D_{\text{h}}}$)	1.48×10^4 to 4.95×10^5
Stack	Number of cell (N_{cell})	51
	Anode stoichiometry (ζ_{A})	1.2
	Cathode stoichiometry (ζ_{C})	2.0
	Current density (J)	0.5 A s^{-2}
Electrode backing	Thickness (δ)	2.5×10^{-4} m
	Porosity (ϕ)	0.4
Catalyst layer	Thickness (δ_{c})	2.0465×10^{-5} m
Membrane	Thickness (δ_{m})	1.64×10^{-4} m

(a)

(b)
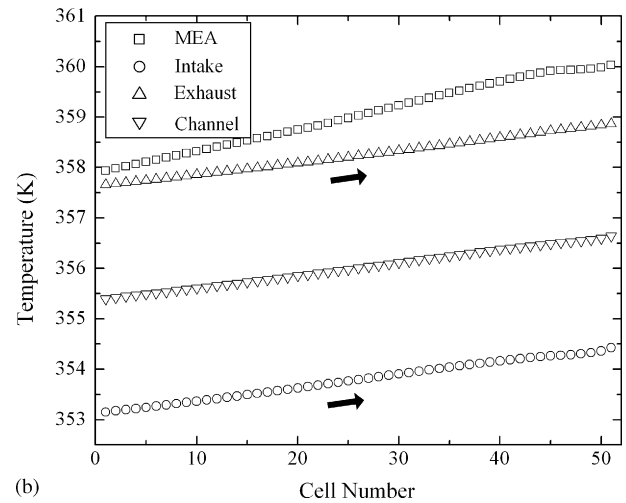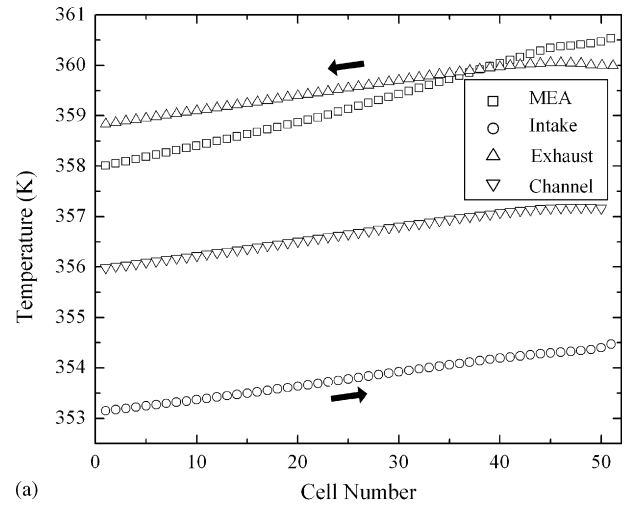
Fig. 5. Typical temperature distributions of the MEA and coolant streams along the intake and exhaust manifold as well as the average temperature in the flow channel for a fuel cell stack; $D_h = 20$ mm, $d_h = 0.75$ mm, $Q_{\text{w}} = 1.42 \times 10^{-4}$ m^3 s^{-1}. (a) U configuration and (b) Z configuration.

Substituting into Eq. (16) for $Q_{i,j}$ and keeping the terms up to the first order about ΔQ_i yields:

$$\Delta P_{i,j} = \theta_{i,j} r_{1,i,j} Q_{i,j,\text{prev}}^{n_{i,j}} + \theta_{i,j}(r_{2,i,j} + r_{3,i,j}) Q_{i,j,\text{prev}}$$
$$+ \theta_{i,j} \Delta Q_i [n_{i,j} r_{1,i,j} Q_{i,j,\text{prev}}^{n_{i,j}-1} + (r_{2,i,j} + r_{3,i,j})] \quad (39)$$

Substituting this expression into Eq. (8) we have

$$\Delta Q_i = \frac{\sum_{j=1}^{N_{ls}} \theta_{i,j}(r_{1,i,j} Q_{i,j,\text{prev}}^{n_{i,j}} + (r_{2,i,j} + r_{3,i,j}) Q_{i,j,\text{prev}})}{\sum_{j=1}^{N_{ls}} \theta_{i,j}(n_{i,j} r_{1,i,j} Q_{i,j,\text{prev}}^{n_{i,j}-1} + (r_{2,i,j} + r_{3,i,j}))} \quad (40)$$

Then Eqs. (13)–(17), (38) and (40) are solved iteratively until the summation of Eq. (39) around a closed loop i converges within a preset tolerance, which is less than 10^{-3} Pa in every loop segment.

After reaching a converged solution for flow solver, the amount of heat transfer to each stream is determined in association with the flow rates and heat generation in each cell as described in the previous section. Then temperature, pressure and species concentrations are sent to the fuel cell model to obtain output voltage of each cell. All material properties are

renewed according to the temperature and pressure for the next iteration. The iteration is carried out until the maximum difference of the each cell voltage from the value of previous iteration is less than 10^{-5} V.

4. Results and discussion

In the present study, analysis has been carried out for a PEM fuel cell stack which consists of 51 cells with 144 cm^2 active cell area. The current density is fixed at 0.5 A cm^{-2} generating about 2 kW as output power. Table 2 lists the dimensions, properties, and operating conditions in the present study. A total of five and seven different sizes for the manifold and flow channel designs with nine different coolant flow rates have been considered. This resulted into a total of 630 cases investigated, or 315 cases for each of the U and Z stack configurations. For each case, it took about 30 min of computation time in a Linux PC cluster built by 10 P-4 CPUs with 20 GB of main memory. This indicates that the present numerical algorithm is very
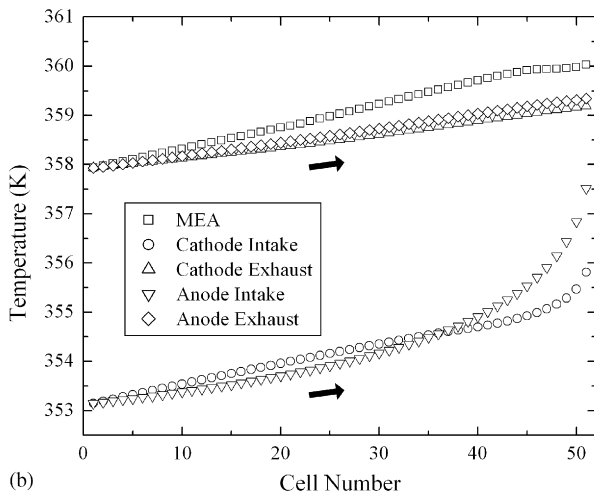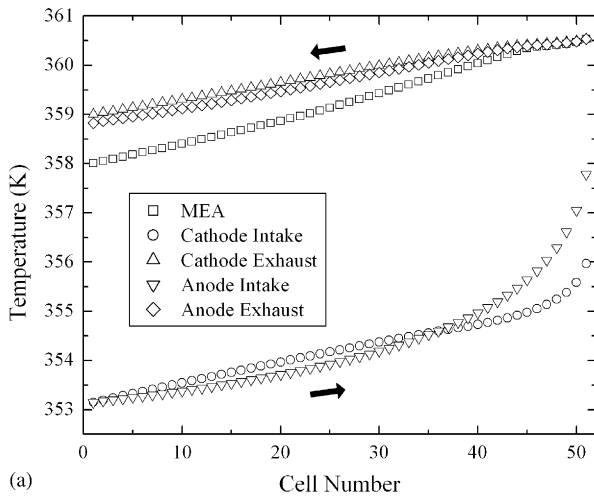

Fig. 6. Temperature distributions of the gas streams in anode and cathode stack manifolds; $D_h = 20$ mm, $d_h = 0.75$ mm, $Q_w = 1.42 \times 10^{-4}$ m^3 s^{-1}. (a) U configuration and (b) Z configuration.
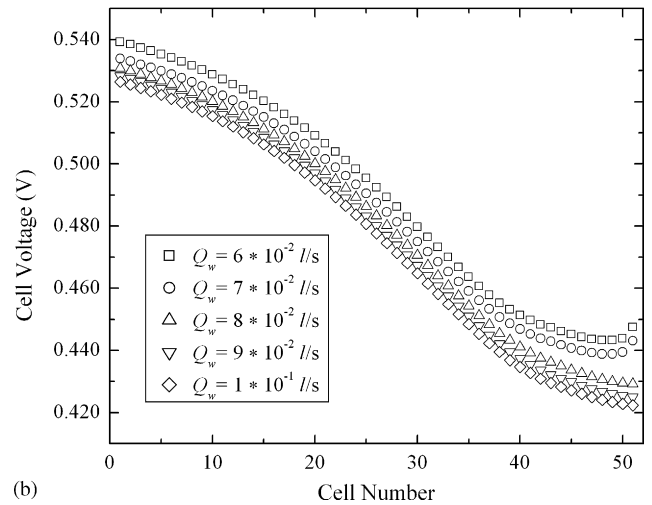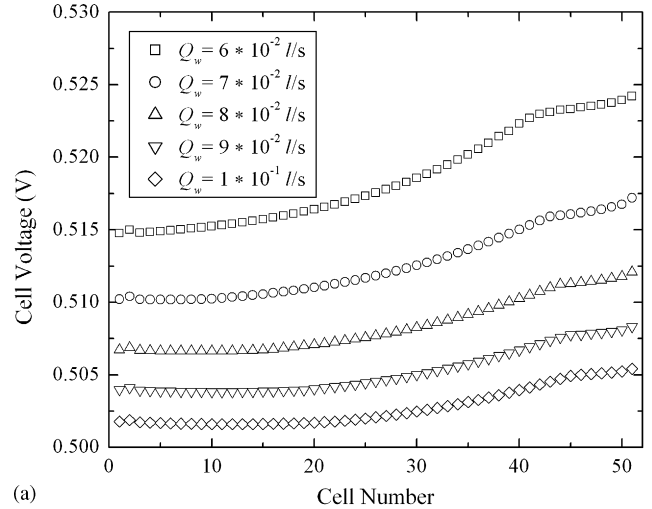

Fig. 7. Voltage distributions in U configuration fuel cell stack for various coolant flow rates: $Q_w = 0.85 \times 10^{-4}$–$2.84 \times 10^{-3}$ m^3 s^{-1} ($Re_{D_h} = 1.48 \times 10^4$–$4.95 \times 10^5$). (a) Design A: $D_h = 20$ mm and $d_h = 0.75$ mm and (b) design B: $D_h = 12.5$ mm and $d_h = 2.0$ mm.

computationally efficient for a stack of this size, and is useful for practical stack design calculations. Section 4.1 presents the flow and temperature distributions for a typical operating condition and their effects on stack performance. Then, in Section 4.2, stack optimization study is presented based on the net stack power.

4.1. Effect of flow and temperature distribution

Flow non-uniformity among the cells in a stack is known to induce performance degradation of fuel cell stacks [26,28]. Sufficient flow uniformity can be ensured by enlarging manifold diameter so that the manifold behaves like a plenum, however it is limited by the size of bipolar plate. The individual cell performance also depends on the cell temperature which is controlled by the coolant flow rate in a fuel cell stack.

Analysis has been carried out for two common stack designs: U and Z configurations. The inlet and outlet of the stack manifold are located at the first cell in case of the U configuration while the outlet of Z configuration is located at the last cell. A typical temperature distribution of the MEA and coolant streams for the U and Z configuration stacks is shown in Fig. 5. The inlet temperature of the coolant, anode and cathode streams are fixed at 353.15 K (80 °C) in this study. The temperature of the coolant stream gradually increases along the intake manifold. The majority of the temperature rise occurs as the coolant passes through the flow channels on the cooling plate, due to the heat transfer from the MEA. In the exhaust manifold, the temperature for the U stack configuration seems to decrease along the flow direction since the coolant temperature out of each cell is higher at upstream of the exhaust manifold. The temperature of the coolant stream can exceed that of the MEA due to the heat transfer and increasing mass flow rate along the exhaust manifold. The temperature distribution for the Z configuration, however, increases along the flow direction, with almost the same outlet temperature. A comparison reveals that the MEA temperature for the U configuration is slightly higher than that for the Z configuration. Because of the difference for the flow direction in the exhaust manifold, U configuration results in the temperature in the exhaust manifold being higher than the MEA for the majority of the cells in the stack; while for the Z configuration the temperature in the exhaust is always less than the MEA temperature.

The temperature distributions of the gas streams in the anode and cathode stack manifold are similar to those of the coolant stream, as shown in Fig. 6. The rate of the temperature increment of the cathode stream is higher for a significant number of cells in the stack than that of the anode stream since the cathode stream is turbulent at the inlet of the intake manifold resulting in a larger Nusselt number. However, near the end of the intake manifold, the temperature of the anode gas stream increases faster compared to the cathode stream, because of rapidly decreasing mass flow rate of the anode stream there. The amount of heat transfer to the gas streams is found to be 3.2 W for the anode stream and 20.4 W for the cathode stream while the total amount of heat generation is 3480.5 W, compared to the stack electrical power output of 1916.1 W.

Fig. 7 shows the cell voltage distributions in two distinct designs of U configuration as a function of the coolant flow rates. In Fig. 7(a), the cell voltage increases along the stack while it decreases in Fig. 7(b). This trend is more apparent for lower coolant flow rates. For the stack design A, it has a small flow channel diameter ($d_h = 0.75$ mm) and relatively large manifold diameter ($D_h = 20$ mm), and is hence characterized by high flow uniformity. On the other hand, the flow uniformity is low for the stack design B since it has a large flow channel diameter ($d_h = 2$ mm) and relatively small manifold diameter ($D_h = 12.5$ mm). The temperature effect is dominant in Fig. 7(a) due to high flow uniformity and this trend is similar for the Z configuration shown in Fig. 8(a). The flow transition from turbulent to laminar flow is responsible for the change in the slope of the cell voltage and temperature profiles for cell numbers above 40 shown in Fig. 7(a). The voltage decrement in Fig. 7(b) is attributed to the effect of flow variances along the intake manifold caused by the lower flow uniformity of design B.

Different from the design B for the U configuration, the voltage profile of the design B for the Z configuration shows a local minimum around the middle of the stack by the combined effect of temperature and concentrations. This phenomenon is caused by the different pressure distribution for the Z configuration as
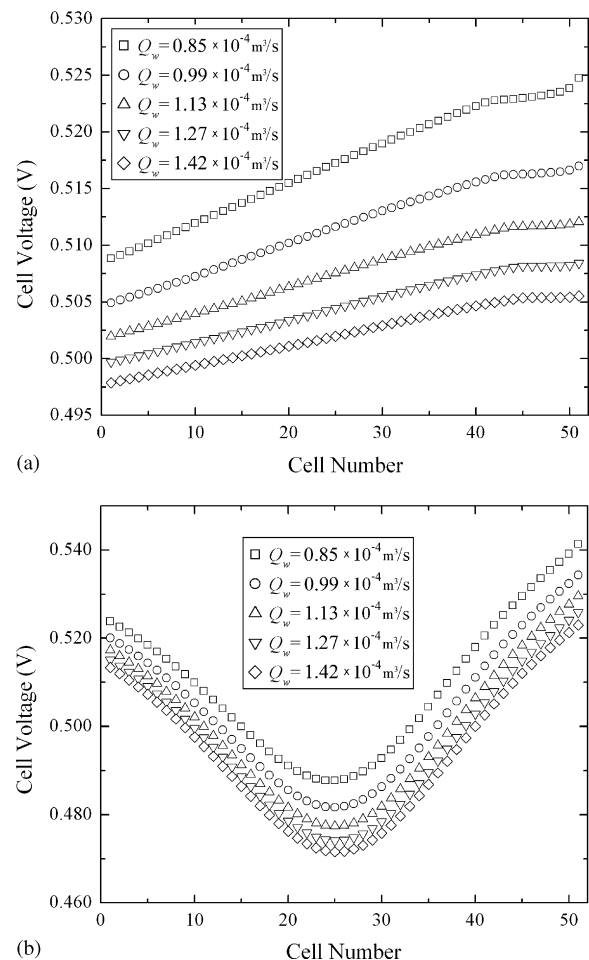

(a)

(b)

Fig. 8. Voltage distributions in Z configuration fuel cell stack for various coolant flow rates: (a) $D_h = 20$ mm, $d_h = 0.75$ mm, (b) $D_h = 12.5$ mm, $d_h = 2.0$ mm.
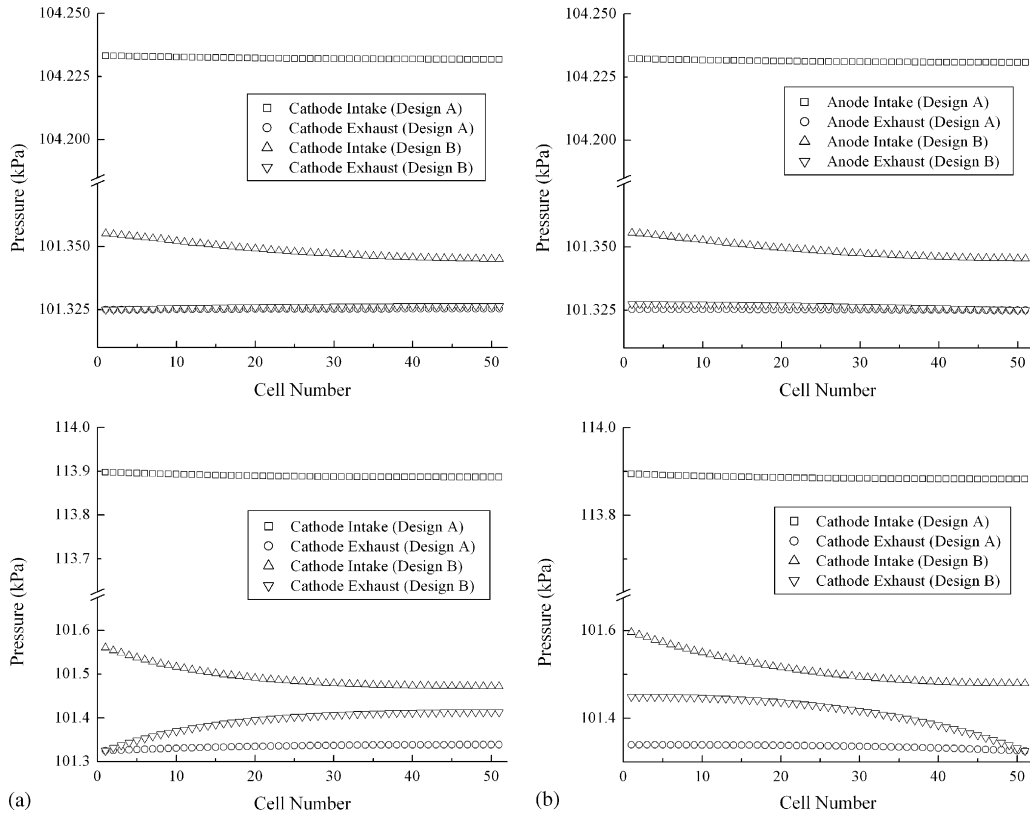
Fig. 9. Pressure distributions in anode and cathode manifolds; (a) anode (U configuration), (b) anode (Z configuration), (c) cathode (U configuration), (d) cathode (Z configuration); $Q_w = 1.42 \times 10^{-4}$ m^3 s^{-1}; design A: $D_h = 20$ mm and $d_h = 0.75$ mm; design B: $D_h = 12.5$ mm and $d_h = 2.0$ mm.

shown in Fig. 9. High flow uniformity is characterized by high average pressure and low pressure drop in the intake manifold, resulting in low concentration variation in anode and cathode flow channels for design A. However a different distribution is observed in the exhaust manifold due to different exit positions, i.e. the pressure increases with the cell number for the U configuration while decreases for the Z configuration. This results in the pressure difference having a minimum near the middle of the Z configuration, which is more evident for the cathode manifolds.

To clarify the effect of the flow and temperature distributions on the stack performance, the distributions of temperature, species concentration, and stoichiometry in the anode and cathode manifolds are shown in Fig. 10. The MEA temperature is also affected by the uniformity of the flow in the gas flow channels. The small differences in the cell inlet temperature $T_{i,\text{in}}$ caused by the degradation of flow rates in the anode and cathode flow channels are accumulated along the intake manifold, resulting into a clear temperature difference for the last few cells. The pressure distribution in the anode and cathode streams are considerable for the design B due to the lower flow uniformity, which leads to a considerable concentration variations for design B in Fig. 10. As a result, the cell voltage distributions for design A in Figs. 7 and 8 resemble the temperature distributions in Fig. 10 when the effects of concentration distribution are diminished. On the other hand, voltage distributions for design B in Figs. 7 and 8 are similar to that of oxygen concentration in the cathode in Fig. 10. The effect of concentration degradation in

cathode is dominant since the majority of the voltage loss occurs in cathode [27].

From the above discussion, it becomes clear that a uniform voltage distribution for the cells in a stack could be achieved without a uniform distribution of the reactant flows and temperature—a condition difficult to achieve. For example, by examining the effect of flow and temperature distribution, as shown in Fig. 7 for the U stack configuration, the temperature distribution will increase the cell voltage along the stack, while the flow non-uniformity will cause the cell voltage to decrease along the stack. Then a judicially selected distribution of the reactant flows and temperature along the stack could balance their respective effect so that a uniform cell voltage might be achieved. This provides a new approach to optimal stack design.

4.2. Optimization of manifolds and flow channel designs

In the previous section it is shown that the cell voltage is affected by the distribution of the reactant gas flows and temperature. The effect of flow variation can be minimized by ensuring sufficient flow uniformity through an enlarged manifold and reduced flow channel sizes. However excessively small flow channels can lead to excessive pumping power required to drive the reactant gas flow, in addition to other problems such as manufacturing difficulty. The cell voltage is increased with increasing temperature but a PEM fuel cell stack cannot be operated at much higher than 80 °C. Optimal performance of a PEM fuel cell stack
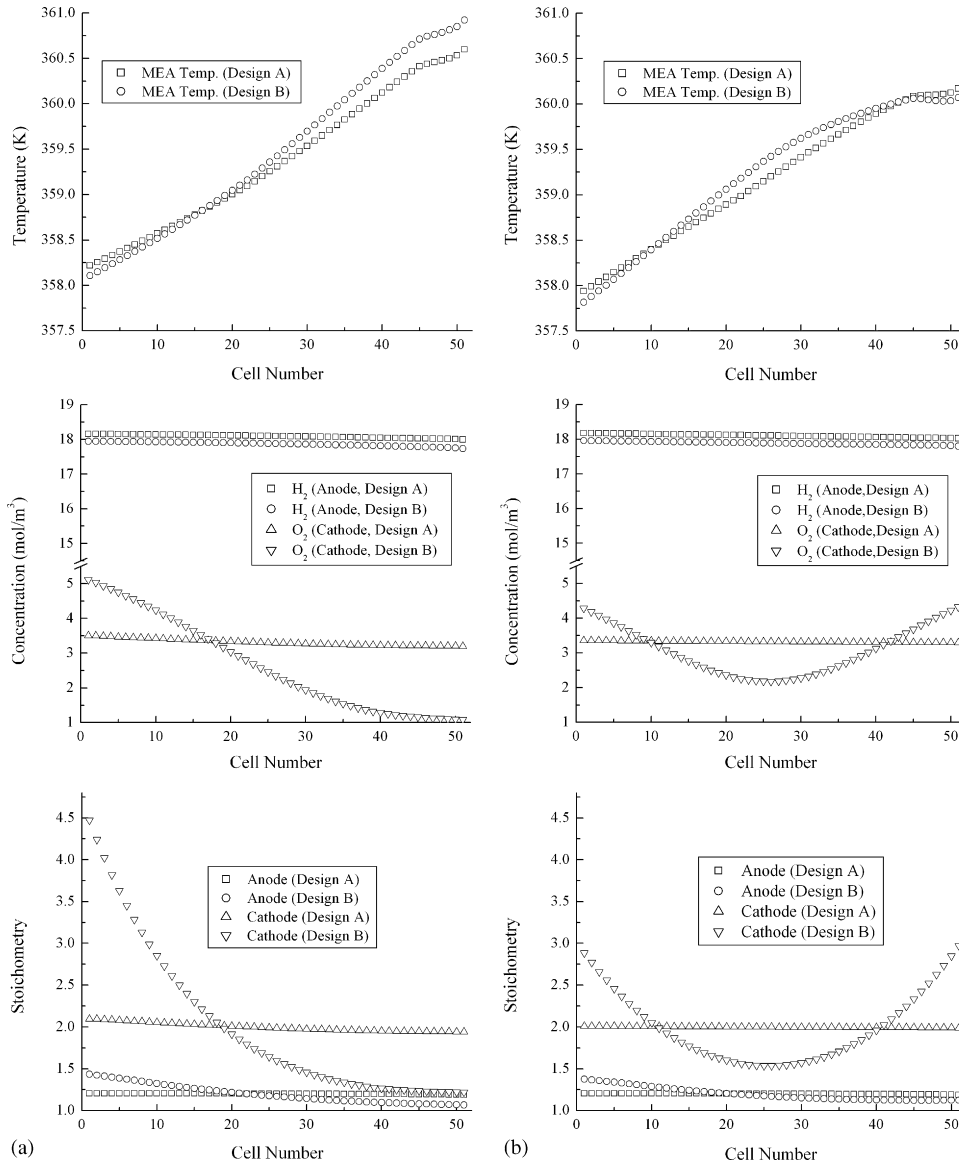
Fig. 10. MEA temperature, species concentration and stoichiometry distributions in anode and cathode manifolds; (a) U configuration and (b) Z configuration; $Q_w = 1.42 \times 10^{-4}\,\mathrm{m^3\,s^{-1}}$; design A: $D_h = 20\,\mathrm{mm}$ and $d_h = 0.75\,\mathrm{mm}$; design B: $D_h = 12.5\,\mathrm{mm}$ and $d_h = 2.0\,\mathrm{mm}$.

can be achieved by optimizing the size of the manifold and flow channel as well as the coolant flow rate.

Fig. 11 presents the effect of coolant flow rate on the average MEA temperature, average cell voltage, pumping power and net stack output power for the designs A and B. The pumping power is calculated as the volumetric flow rate times the amount of pressure drop in each stream. The average temperature of the MEA decreases as the coolant flow rate increases and it is likely to converge to the inlet coolant temperature. The effect of stack design on the average temperature of MEA is observed although it becomes smaller with increased coolant flow rate. The high flow uniformity with higher species concentrations in design A results in a higher cell voltage compared to that of design B for both U and Z configurations. However the design A demands more pumping power especially for the cathode gas streams. The total net pumping power can be found according to the coolant flow rate since the pumping powers for the

anode and cathode are already determined from the inlet stoichiometries and total pressure drop for the given configuration. The reasonable range for the coolant flow rate may vary from 0.85×10^{-4} to $3.0 \times 10^{-3}\,\mathrm{m^3\,s^{-1}}$. Maximum temperature of the MEA reaches 373.15 K (=100 °C) when the coolant flow rate is less than $0.8 \times 10^{-4}\,\mathrm{m^3\,s^{-1}}$.

Fig. 12 shows a three dimensional plot of the net stack power for wide ranges of manifold and flow channel diameters. The individual surface plot represents the result for a given coolant flow rate and it exhibits major dependency on the flow channel diameter. The variance of the net power with respect to the flow channel diameter becomes less considerable for the larger manifold diameter. For each cooling flow rate, there exists an optimal flow channel diameter for which the net stack power achieves a maximum value. Low flow uniformity is responsible for the power degradation at large flow channel diameters while, at small flow channel diameters, the net stack power is
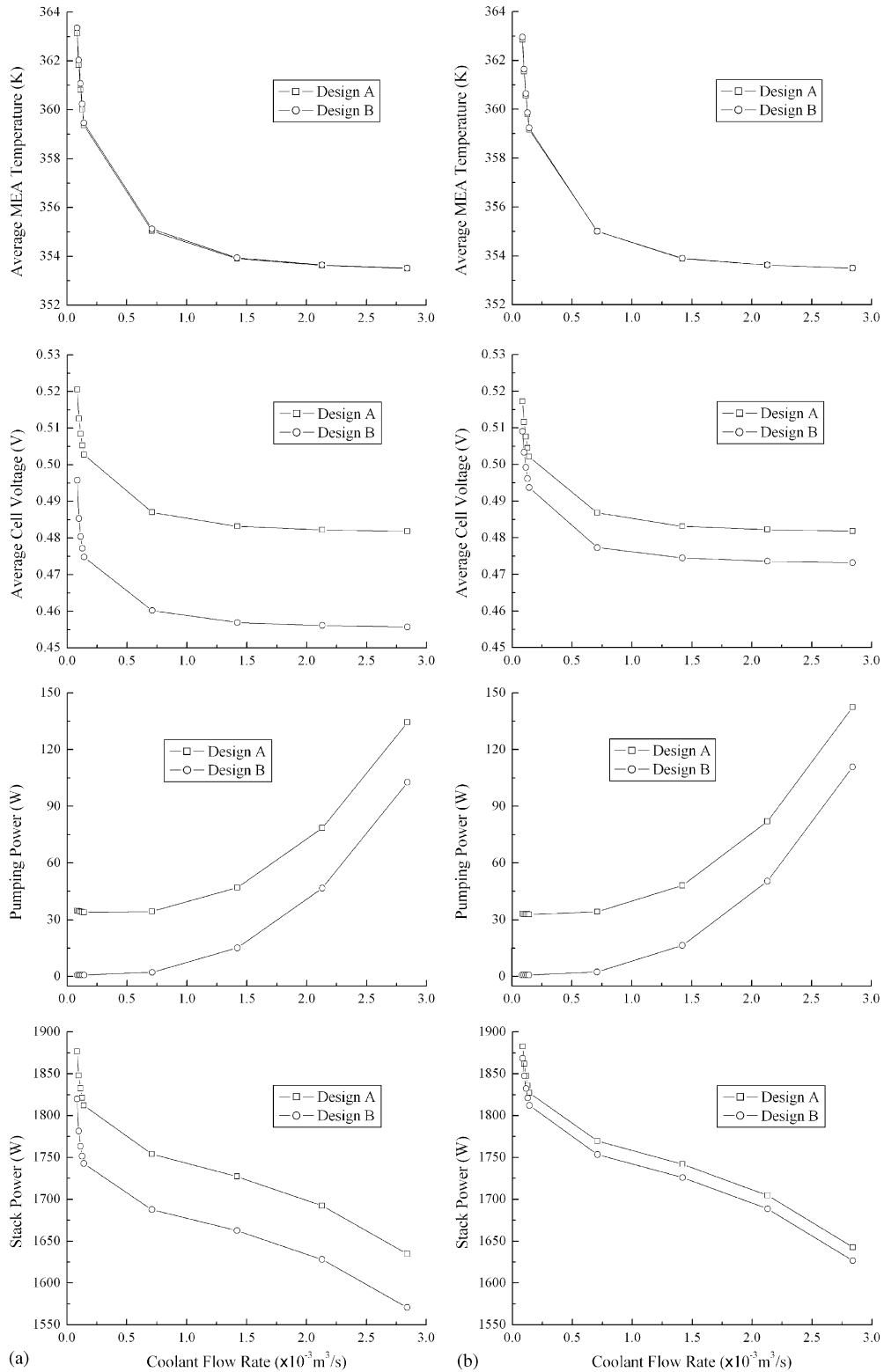
Fig. 11. Average MEA temperature, average cell voltage, total pumping power and net stack power according to various coolant flow rate. (a) U configuration and (b) Z configuration; $Q_w = 1.42 \times 10^{-4}$ m^3 s^{-1}; design A: $D_h = 20$ mm and $d_h = 0.75$ mm, design B: $D_h = 12.5$ mm and $d_h = 2.0$ mm.

deteriorated by the excessive pumping power. It is also seen that the stack power increases as the coolant flow rate is decreased because of higher average cell temperature. In Fig. 13, the net stack power is compared between the U and Z configurations

for various coolant flow rates. The maximum net stack power is obtained when the manifold and flow channel diameters are 20 and 1.5 mm (design A in Fig. 13), respectively. Although it is not considerable, the maximum net power of U configuration is
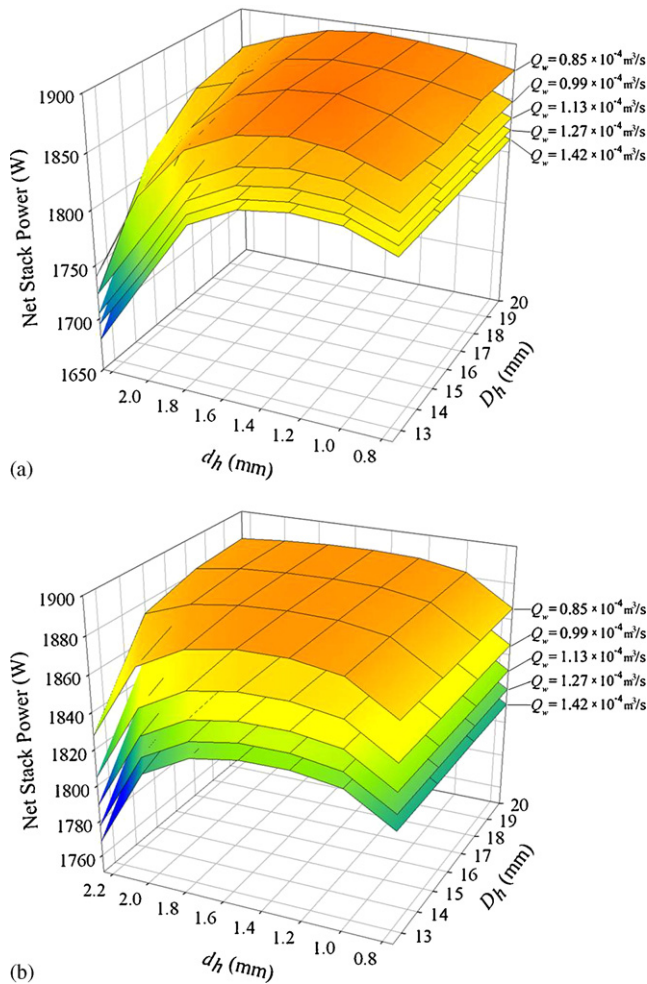
Fig. 12. A three-dimensional plot of the net stack power for various stack designs and coolant flow rates ($Re_{D_h} = 1.48 \times 10^4$–$4.95 \times 10^5$). D_h = 12.5–20 mm, and d_h = 0.75–2.25 mm. (a) U configuration and (b) Z configuration.
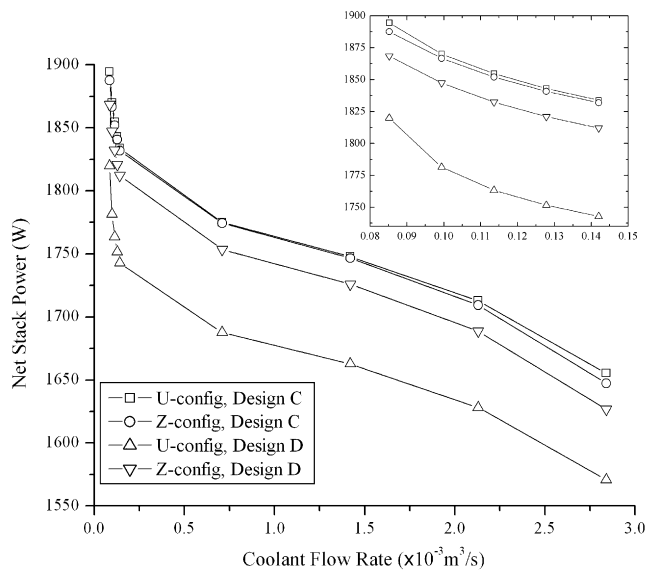

Fig. 13. Comparison of the net stack power between U and Z configurations for various coolant flow rates; design A: D_h = 20 mm and d_h = 1.5 mm; design B: D_h = 1.25 mm and d_h = 2.0 mm.

slightly higher than that of Z configuration for the entire range of the coolant flow rates investigated. On the other hand, the net power for the U configuration is reduced considerably when the flow uniformity is poor such as for design B shown in Fig. 13. The effect of flow variance on net stack power is much less for the Z configuration since it has higher flow uniformity than the U configuration for the same inlet conditions as shown in Fig. 10. The Z configuration is hence preferable when the sufficient flow uniformity cannot be ensured.

5. Conclusions

In this study, a non-isothermal stack model has been developed for PEM fuel cells, and the effect of reactant flows and temperature distribution on the stack performance has been analyzed. It is shown that the flow and temperature distribution have a different influence, and a judicial matching of their distribution can provide the ideal uniform cell voltage distribution. Optimal stack design for the maximum net stack power has also been investigated through minimizing performance degradation and excessive pumping power. The effect of flow distribution on the stack performance is found to be considerably less for the Z configuration.

Acknowledgement

References

[1] J. Hamelin, K. Agbossou, A. Laperriere, F. Laurencelle, BoseF T., Int. J. Hydrogen Energy 26 (6) (2001) 625–629.
[2] J. Baschuck, X. Li, Int. J. Energy Res. 28 (2004) 697–724.
[3] A. Bıyıkoglu, Int. J. Hydrogen Energy 30 (2005) 1181–1212.
[4] D. Chu, R. Jiang, C. Walker, J. Appl. Electrochem. 30 (2000) 365–370.
[5] V. Gurau, H. Liu, S. Kakac, AICHE J. 44 (1998) 2410–2422.
[6] T. Berning, D.M. Lu, N. Djilali, J. Power Sources 106 (2002) 284–294.
[7] S. Um, C.Y. Wang, K.S. Chen, J. Electrochem. Soc. 147 (2000) 4485–4493.
[8] S. Dutta, S. Shimpalee, J.W. Van Zee, J. Appl. Electrochem. 30 (2000) 135–146.
[9] N.P. Siegel, M.W. Ellis, D.J. Nelson, M.R. von Spakovsky, J. Power Sources 115 (2003) 81–89.
[10] S. Mazumder, J.V. Cole, J. Electrochem. Soc. 150 (2003) A1503–A1509.
[11] H. Meng, C.Y. Wang, J. Electrochem. Soc. 151 (2004) A358–A367.
[12] H. Meng, C.Y. Wang, Fuel Cells 5 (2005) 455–462.
[13] H. Ju, H. Meng, C.Y. Wang, Intl J. Heat Mass Transfer 48 (2005) 1303–1315.
[14] H. Meng, C.Y. Wang, Chem. Eng. Sci. 59 (2004) 3331–3343.
[15] S. Shimpalee, S. Greenway, D. Spuckler, J.W. Van Zee, J. Power Sources 135 (2004) 79–87.
[16] Y. Wang, C.Y. Wang, J. Power Sources 153 (2006) 130–135.
[17] S. Mazumder, J.V. Cole, J. Electrochem. Soc. 150 (2003) A1510–A1517.
[18] H. Meng, C.Y. Wang, J. Electrochem. Soc. 152 (2005) A1733–A1741.
[19] H. Ju, C.Y. Wang, J. Electrochem. Soc. 151 (2004) A1954–A1960.
[20] H. Ju, C.Y. Wang, S. Cleghorn, U. Beuscher, J. Electrochem. Soc. 152 (2005) A1645–A1653.
[21] S. Um, C.Y. Wang, J. Power Sources 156 (2006) 211–223.
[22] A.A. Kulikovsky, J. Electrochem. Soc. 150 (2003) A1432–A1439.
[23] Y. Wang, C.Y. Wang, J. Electrochem. Soc. 152 (2005) A445–A453.
[24] A. Rowe, X. Li, J. Power Sources 102 (2001) 82–96.

[25] D. Thirumulai, R. White, J. Electrochem. Soc. 144 (5) (1997) 1717–1723.

[26] T. Nguyen, R. White, J. Electrochem. Soc. 140 (8) (1993) 2178–2186.

[27] J. Baschuk, X. Li, Int. J. Global Energy Issues 20 (3) (2003) 245–276.

[28] G. Karimi, J.J. Baschuk, X. Li, J. Power Sources 147 (1–2) (2005) 162–177.

[29] G. Maggio, V. Recupero, C. Mantegazza, J. Power Sources 62 (2) (1996) 167–174.

[30] D. Patel, H. Maru, M. Farooque, C. Ware, J. Electrochem. Soc. 131 (12) (1992) 2750–2756.

[31] J. Kim, S. Supramaniam, C.E. Chamberlin, J. Electrochem. Soc. 142 (8) (1995) 2670–2674.

[32] J. Lee, T. Lark, J. Power Sources 73 (2) (1998) 229–241.

[33] F. Barbir, B. Balasubrumanian, J. Neutzler, Proceedings of the ASME Advanced Energy Systems Division, The American Society of Mechanical Engineers, New York, 1999, pp. 305–315.

[34] I.E. Idelchik, Handbook of Hydraulic Resistance, 3rd ed., CRC Press, Boca Raton, 1994.

[35] F.P. Incropera, D.D. Witt, Introduction to Heat Transfer, 2nd ed., Wiley, New York, 1990.

[36] H. Cross, Univ. Illinois Bull. 286 (1936).